Chemical Engineering Journal 362 (2019) 53–62

Contents lists available at ScienceDirect

Chemical Engineering Journal

journal homepage: www.elsevier.com/locate/cej

Hierarchical Fe-ZSM-5/SiC foam catalyst as the foam bed catalytic reactor (FBCR) for catalytic wet peroxide oxidation (CWPO)

Xiaoxia Ou[a,1], Fotios Pilitsis[a,1], Yilai Jiao[a,b], Yong Zhang[c], Shaojun Xu[a], Martin Jennings[d], Yi Yang[c], S.F. Rebecca Taylor[a], Arthur Garforth[a], Huiping Zhang[c], Christopher Hardacre[a,*], Ying Yan[c,*], Xiaolei Fan[a,*]

[a] School of Chemical Engineering and Analytical Science, The University of Manchester, Oxford Road, Manchester, United Kingdom
[b] Shenyang National Laboratory for Materials Science, Institute of Metal Research, Chinese Academy of Sciences, 72 Wenhua Road, Shenyang 110016, China
[c] School of Chemistry and Chemical Engineering, South China University of Technology, Guangzhou, Guangdong 510640, China
[d] School of Chemistry, The University of Manchester, Oxford Road, Manchester, United Kingdom

HIGHLIGHTS

- Hierarchical Fe-ZSM-5/SiC catalyst prepared by chemical vapour deposition (CVD).
- Structured foam bed reactors (FBRs) for catalytic wet peroxide oxidation (CWPO).
- Detailed analysis of hydrodynamics of FBRs by pulse response experiments.
- Good longevity and performance of Fe-ZSM-5/SiC catalyst under flow conditions.

GRAPHICAL ABSTRACT

Hierarchical Fe-ZSM-5/SiC catalyst as structured reactors for catalytic wet peroxide oxidation, showing good longevity and performance under flow conditions.

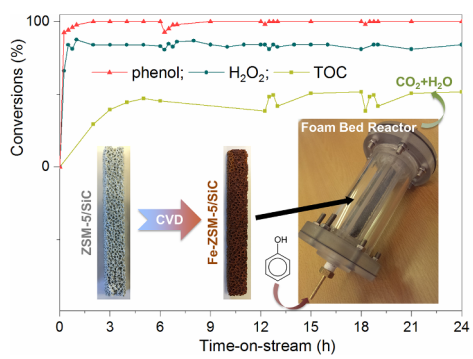

ARTICLE INFO

Keywords:
SiC foam
Structured catalyst
Chemical vapour deposition (CVD)
Catalytic wet peroxide oxidation (CWPO)
Macromixing

ABSTRACT

Structured Fe-ZSM-5 zeolite supported on silicon carbide (SiC) foam catalyst was develop and applied as the packed foam bed catalytic reactor (FBCR) to the liquid phase catalytic wet peroxide oxidation (CWPO) of phenol under flow conditions. Fe catalysts were uniformly incorporated into ZSM-5 coatings using chemical vapour deposition (CVD). Fluid flow analysis of FBCR was performed by varying liquid flow rate, showing the transition of reactor type from the plug flow reactor to the continuous stirred tank reactor at about 1 ml min^{-1}. Systematic investigation of CWPO within Fe-ZSM-5/SiC FBCRs identified the optimum condition of operating the FBCR (80 mm bed length) as at 60 °C and 1 ml min^{-1} with the turnover frequency (TOF) of 95 h^{-1} for phenol degradation (apparent activation energy = 3.4 kJ mol^{-1}) and total organic carbon (TOC) conversion of 45.5%. It

* Corresponding authors.
E-mail addresses: c.hardacre@manchester.ac.uk (C. Hardacre), yingyan@scut.edu.cn (Y. Yan), xiaolei.fan@manchester.ac.uk (X. Fan).
[1] These authors contributed equally to this work.

https://doi.org/10.1016/j.cej.2019.01.019
Received 22 July 2018; Received in revised form 2 January 2019; Accepted 4 January 2019
Available online 04 January 2019

was believed that the enhanced macromixing promoted by cellular foam supports was accountable for the observed catalytic performance. The longevity of FBCR under flow conditions was also assessed, showing its good stability over 24 h, as well as the potential for practical adoption.

1. Introduction

The increasing industrial activity of modern society has raised issues concerning environmental pollution. Many processes produce organic waste ending up on the atmosphere, soil and waterways, endangering all forms of life. One class of organic pollutants that is vastly produced by various industrial processes, such as oil refining, petrochemical and polyolefines processing, textile and leather processing industries [1], referring to phenolic compounds. Quantitatively, 70,190 tons per annum of phenol are produced in European territory (exposure limit: $< 20\,mg\,m^{-3}$), which has a relatively low degradation rate constant of $0.05\,d^{-1}$ in surface waters. Low doses of 140–290 mg phenol kg^{-1} through the oral route, or dermal exposure could be lethal for humans due to its fast adsorption through tissues [2].

Destructive methods for phenol treatment include biological (*e.g.* biodegradation which is lengthy), thermal (*e.g.* incineration which is energy intensive) and chemical treatment (*e.g.* advanced oxidation processes, AOP), among which AOPs using ozone (O_3), hydrogen peroxide (H_2O_2) and/or UV light stand out as a continuous progression, showing high efficiency in mineralisation of organic pollutants [3,4]. Catalytic wet peroxide oxidation (CWPO) processes employ eco-friendly non-toxic H_2O_2 and hold good promise for potential applications in practical settings [5–9] since gas-to-liquid mass transfer (for O_3) and special reactor configuration (for UV) can be avoided. In CWPO, excessive H_2O_2 is usually used to ensure the complete mineralisation of organics into CO_2 and H_2O under mild conditions [10], for example, 14 mol of H_2O_2 are needed to mineralise one-mole phenol fully. H_2O_2 is catalytically decomposed to produce hydroxyl radicals, which has a very high oxidation potential (+2.8 V at pH 0) and high O–H bond energy (109 kcal mol^{-1}) [10], virtually being able to oxidise any organic pollutants. Heterogeneous CWPOs with iron-based catalysts have the potential benefits of taking advantage of the Fenton process (of fast production of hydroxyl radicals [11]) and overcoming the problem of recovery, regeneration and reuse of catalysts [5,12].

To avoid the separation of active species from the CWPO processes, supported heterogeneous catalysts are preferred over homogeneous counterparts, in which porous supports, such as pillared clays [13,14], activated carbon [9,15], alumina [16,17] and zeolites [6,7,18,19], are commonly used to disperse active species. For example, ZSM-5 zeolite was employed to support iron (Fe) catalysts for CWPO of phenol [5,8,20–25] due to its high specific surface area (*ca.* 350–400 $m^2\,g^{-1}$) [26] and good oxidation resistance (against the oxidising environment in CWPO) [27].

Packed bed configurations employing catalyst pellets generally showed the good performance of CWPO at laboratory scales [5–7]. For example, Fe_2O_3/SBA-15 [7], Fe-ZSM-5 and Fe_2O_3/MCM-41 [5,6] were used in packed beds and achieved high conversions of phenol and total organic carbon (TOC) (*i.e.* phenol conversion > 99% and TOC conversion > 66%).

However, the pressure drop issue of conventional packed bed configurations makes their practical applications challenging, especially handling liquid phase reactions at scales. To prepare a packed bed, pelletisation is needed to transfer powder catalysts into granules, spheres and extrudates [27], in which the use of inert binders, as well as the excessive shaping pressure, may result in the compromised catalytic activity. In addition, the maldistribution of reacting flows through packed bed reactors may also decrease the catalyst efficiency [28].

Recently, structured catalysts/reactors, such as zeolite coatings on paper-like sintered stainless steel fibres [21,29], monolithic reactors [30] and structured cellular foams [31–33], have been recognised as one of the enablers for the process intensification under continuous-flow regimes [34], especially laminar flows [35], which makes them promising candidates for further exploration/exploitation of CWPO processes [36].

Solid open-cell cellular foams (based on base materials of polyurethane, carbon [37,38] and silicon carbide, SiC [39]) were proposed to develop flow-through reactors for environmental catalytic applications, especially photocatalytic treatment of chemical and biological pollutants in gas or liquid phase. Benefiting from features of the cellular structure, such as static mixer effect, high surface-to-volume ratio, low-pressure drop and high transparency to light [39], as well as properties of the base SiC (*e.g.* the semiconductive property [40]), SiC foams could be promising candidates for performing continuous-flow environmental catalysis. More importantly, SiC foam has gained the success at scales and demonstrated the possibility of industrial use [41]. For example, SiC foams have been used as distillation trays at pilot scale and outperformed the conventional trays regarding all key performance indicators [42].

The surface decoration of SiC foams using zeolites (*e.g.* ZSM-5 and SAPO-34) [33,43–47] and metal oxides (*e.g.* TiO_2 and Al_2O_3) [39,40] is established by extensive research to provide quality coatings on SiC foams for catalysis such as photocatalysis [37,38], Fisher-Tropsch synthesis [48,49] and alcohol-to-olefins (MTO) reactions [33,43,46,50]. Of specific relevance to CWPO, in which ZSM-5 was commonly used to support Fe catalysts [5,8], hierarchical ferrisilicate/SiC foams have been demonstrated feasible to perform CWPO [36].

Impregnation is commonly used to deposit catalysts on structured supports [6,21,51]. However, impregnation is prone to promote the inhomogeneous special distribution of active species across supports and the variation of catalyst sizes [52], which may abate the catalytic performance of the resulting structured catalyst. Recently, chemical vapour deposition (CVD) is shown to disperse catalytically active components on structured supports (*e.g.* LTA zeolite/stainless steel fibres [53]) homogeneously and facilely without requirements of drying and reduction.

In this study, the development of structured catalysts of Fe supported on ZSM-5 coated SiC foam (Fe-ZSM-5/SiC) is presented. Uniform incorporation of Fe catalysts in ZSM-5/SiC supports is achieved by CVD. Fe-ZSM-5/SiC catalyst is used as the foam bed catalytic reactors (FBCRs) and assessed by CWPO with phenol as the model compound under laminar flow conditions. The reaction temperature and flow rate are investigated systematically to understand their effects on the residence time distribution and catalytic performance of FBCRs. The longevity of the developed catalytic system is evaluated as well to assess the catalytic FBCRs for potential practical applications.

2. Experimental

2.1. Chemicals

Chemicals including phenol (for molecular biology, Sigma-Aldrich), hydrogen peroxide (50 wt% in water, Sigma-Aldrich), sodium thiosulfate (99%+, Alfa Aesar), potassium iodide (99.9%, Fisher Scientific), hydrogen chloride (VWR chemicals), starch (0.5%, VWR chemicals) and sodium chloride (99.8%, Sigma-Aldrich) were used as received.

2.2. Preparation of ZSM-5 zeolite supported on SiC foam supports (ZSM-5/SiC)

SiC foam supports with an average cell diameter of *ca.* 0.13 mm and porosity (ε) of 70% (10 × 10 × 80 mm) were used in this work. ZSM-5/SiC was prepared by a dip-coating method (Fig. S1), as previously described in [33] and the average ZSM-5 coating on SiC foams was about

5 wt% (estimated by the weight gain of the support after the dip coating).

2.3. Synthesis of Fe-ZSM-5/SiC by chemical vapour deposition (CVD)

Fe-ZSM-5/SiC catalysts were prepared by a CVD method using iron (III) acetylacetonate (98%, Aladdin Industrial Corporation) as the precursor in a tube furnace (Hefei Kejing Materials Technology Co., Ltd.). Prior to CVD, the iron precursor and ZSM-5/SiC were mixed in a crucible and placed in the tube furnace under nitrogen (N_2, the vacuum was applied to the system to extract air before introducing N_2). The evaporation of the precursor was carried out at 120 °C for 1 h. The system was then heated up to 310 °C (with a ramp rate of 5 °C min^{-1}, held at 310 °C for 2 h) for the deposition of iron species on ZSM-5/SiC to prepare Fe-ZSM-5/SiC catalysts. After CVD, the resulting Fe-ZSM-5/SiC catalyst was calcined at 550 °C for 6 h (in a muffle furnace Nabertherm LE6/11 with P300 controller, ramp rate = 1 °C min^{-1}) prior to the catalytic test.

The quantity of Fe species in Fe-ZSM-5/SiC catalysts was determined by atomic absorption spectroscopy (AAS, Shimadzu AA-6800). Fe-ZSM-5/SiC samples were immersed in 3 wt% HCl solution overnight then solutions were analysed by AAS for the quantitative determination of Fe species. It was estimated that about 0.2 wt% iron species were present in Fe-ZSM-5/SiC catalysts (based on the total weight of the whole structured catalyst of 7.6–8.0 g).

2.4. Characterisation of materials

X-ray diffraction (XRD) patterns of materials were obtained using a Philips X'Pert X-ray diffractometer (CuKα_1 radiation, $\lambda = 1.5406$ Å, 40 kV, 40 mA, $5° < 2\theta < 65°$, 0.0167° step size). X-ray photoelectron spectroscopy (XPS) analysis was carried out on a Kratos AXIS Ultra DLD apparatus equipped with monochromated Al *Kα* X-ray source, a charge neutraliser and a hemispherical electron energy analyser. During data acquisition, the chamber pressure was kept below 10^{-9} mbar and a pass energy of 40 eV. The spectra were analysed using CasaXPS software pack and corrected for charging using C 1s binding energy (BE) as the reference at 284.8 eV. The morphology and quantitative composition analysis of materials were acquired by a Philips XL30 FEG scanning electron microscope (SEM, beam acceleration voltage = 15 kV) equipped with an energy-dispersive (EDS) detector. Nitrogen (N_2) sorption analysis at −196.15 °C was performed using a Quantachrome surface area analyser (Nova 2200). Before N_2 sorption analysis, samples were outgassed at 300 °C overnight. The specific surface area of materials was determined using the Brunauer-Emmett-Teller (BET) method. Pore size analysis was performed using the Barrett-Joyner-Halenda (BJH) method and the desorption branch of isotherms. The meso-/macro-pore sizes of the samples were also analysed using mercury (Hg) intrusion porosimetry on Micromeritics' AutoPore IV 9510 (pressure range: 0.0007–413.6854 MPa).

2.5. Catalytic wet peroxide oxidation (CWPO) of phenol in foam bed catalytic reactors (FBCRs)

CWPO of phenol was carried out in the foam bed catalytic reactor (FBCR loaded with a single Fe-ZSM-5/SiC catalyst of 80 mm length and *ca.* 8.0 g weight, as seen the inset in Fig. 2) under continuous flow conditions and the experimental set-up is shown in Fig. 2. The synthetic analogue of wastewater containing phenol was prepared to have a concentration of 100 mg l^{-1} phenol (C_{phenol}, or part per million, ppm). The system temperature was maintained by circulating isothermal water through the jacket and measured by a thermal couple. To start CWPO, a mixture of phenol solution and H_2O_2 (molar ratio of H_2O_2 to phenol = 14) was fed into the upflow FBCR *via* an HPLC pump (KNAUER P.4.1S). The mixture was preheated (by going through a tube which was immersed in an isothermal water bath) to the required temperature before going into FBCR. The effluent from CWPO was cooled down by an ice bath (to avoid evaporation) then collected for various analyses.

Different temperatures (*T*) of 25, 40 and 60 °C (measured by a thermocouple at the outlet of FBCRs) and flow rates (*F*) of 0.5, 1 and 2 ml min^{-1} were investigated to study the effect of kinetics and hydrodynamics on CWPO. All experiments were carried out under the continuous flow condition for 6 h with internally collected samples for determining concentrations of H_2O_2, phenol, total organic carbon (TOC) and Fe. pH values of effluents were monitored as well using a pH

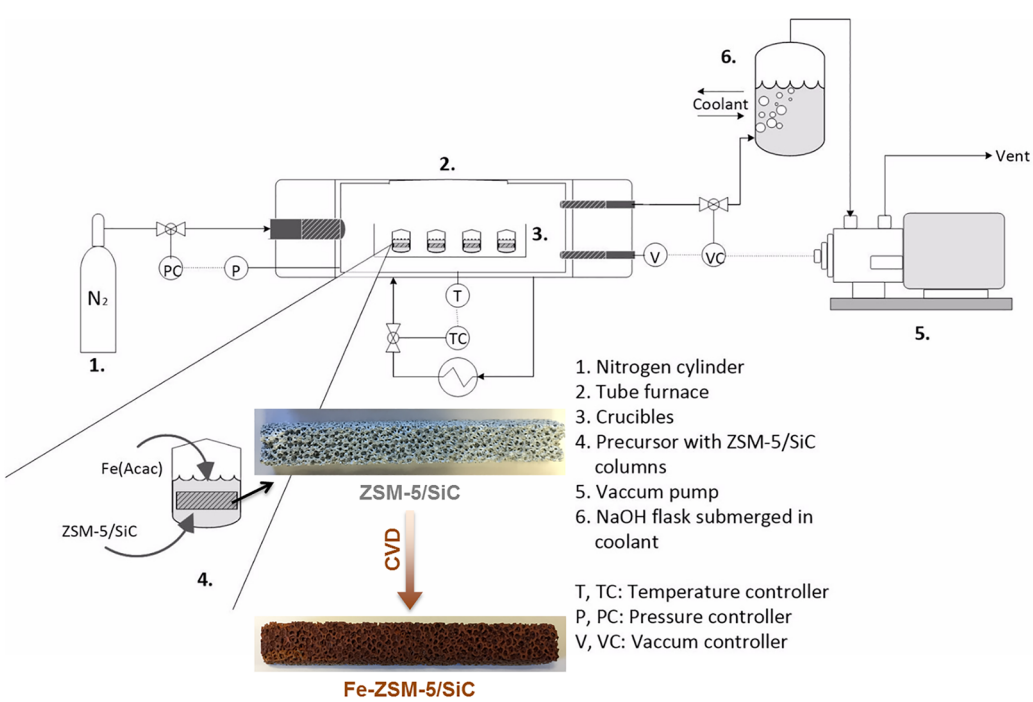

Fig. 1. Schematic diagram of the experimental set-up for the preparation of Fe-ZSM-5/SiC catalysts using CVD method.

meter (HANNA HI 2550). Blank experiments (at 25, 40 and 60 °C) with Fe-ZSM-5/SiC (without H_2O_2) and SiC foam (without ZSM-5 coating) were performed to understand the contribution of adsorption and liquid phase reaction to the measured catalytic performance.

High-performance liquid chromatography (HPLC) was used to analyse concentrations of phenol (Fig. S2) and degradation products in the effluent. HPLC analysis was performed using an Agilent 1220 Infinity LC system equipped with a Diode Array Detector. An Agilent HC-C18(2) column was used for the detection of organics. Relevant HPLC conditions are: wavelength = 210 nm, oven temperature = 30 °C, and sample injection volume = 20 μL, flow rate = 1 ml min^{-1}, mobile phase = ultrapure water and HPLC grade methanol with the volume ratio of 60:40. Calibration of HPLC analysis for phenol and calculation of conversions (phenol, TOC and H_2O_2) are presented in the Supplementary Information (SI). TOC analysis of the effluent was performed on a TOC analyser (TOC-V_{CSH}, Shimadzu). H_2O_2 concentration was determined by the iodometric titration method. Iron leaching from the catalyst during continuous flow operation was measured by inductively coupled plasma optical emission spectrometry (ICP-OES, Thermo iCAP 6000 SERIES, 259.940 nm wavelength). Repeated reactions were performed with catalyst samples from the same synthesis protocols, showing that the conversion values were reproducible to better than ± 10%.

2.6. Pulse response experiments

Residence time distribution (RTD) measurements were performed using the pulse response experiment on FBCR. Deionised water (DI) was continuously flowed through FBCR to achieve steady state, then 2 ml tracer (4 wt% NaCl solution) was injected into the feed stream *via* a tee junction (to ensure that the tracer was inserted as a whole and avoid dispersion in the inlet flow, as indicated in Fig. 2). For each flow rate (*i.e.* F = 0.5, 1 and 2 ml min^{-1}), at least three individual RTD measurements were performed to verify the results. The tracer was injected instantaneously (< 1 s), simulating a Dirac delta function of the concentration. The detection system was composed of a solids detector dipped inside 200 ml of DI, where the effluent stream was discharged.

The detected signal (at every five seconds on stream) was quantified at the ppm scale. The analysis of concentration profiles and RTDs were based on the RTD function ($E(t)$), cumulative distribution function ($F(t)$), average residence time (t_m [min]), theoretical space-time (τ [min]) and variance (σ_t^2 [min^2]) [54], as defined in SI.

3. Results and discussion

3.1. Characterisation of materials

CVD was effective to deposit iron into ZSM-5/SiC support, as shown in Fig. 1, illustrating the colour change of ZSM-5/SiC from chalk white to dark brown after CVD. SEM-EDS elemental mapping of one cross-section of the strut of Fe-ZSM-5/SiC reveals a uniform distribution of Fe across the ZSM-5 coating (Fig. 3). In addition, EDS point analysis at different depths across Fe-ZSM-5 layer (thickness = *ca.* 30 μm) shows comparable Fe concentrations of 7.2, 7.1, 6.6 and 7.2 wt% (local mass fractions of Fe element in the sample), respectively, demonstrating the effectiveness of CVD for loading Fe within the ZSM-5 framework. XRD pattern of Fe-ZSM-5/SiC (Fig. S3) is similar to that of ZSM-5/SiC. Fe species are not identified by XRD analysis which may be due to the overlapped peak positions of iron oxide (2θ = 33.0° and 35.6° [21]) with the SiC phase.

N_2 sorption analysis and Hg intrusion porosimetry (Fig. S4) were performed to understand the textural property of Fe-ZSM-5/SiC catalyst. BET surface area drops from 23.4 m^2 g^{-1} (ZSM-5/SiC) to 19.8 m^2 g^{-1} (Fe-ZSM-5/SiC) after CVD, indicating possible pore blockage by the deposition of Fe species. Meso-/macro-pore size distributions are presented in Fig. 4a with 4 nm mesopores probed by N_2 sorption and *ca.* 95 nm macropores by Hg intrusion. The hierarchical porous system of Fe-ZSM-5/SiC catalysts can be attributed to the inter-crystal/particle pores of the ZSM-5 coating. The presence of meso- and macro-pores in the developed structured catalysts may be beneficial to CWPO in the liquid phase, in which large pores can contribute to mass transfer significantly since the diffusivity of species in the liquid phase is generally five orders of magnitude lower than that in the gas phase [55].

XPS analysis was carried out to understand the chemical state of Fe species in Fe-ZSM-5/SiC catalysts. Fe 2p XPS spectra are complicated to be fitted due to the complex multiplet splitting observed for atoms which contain unpaired electrons. Fe $2p_{3/2}$ portion of the spectrum was

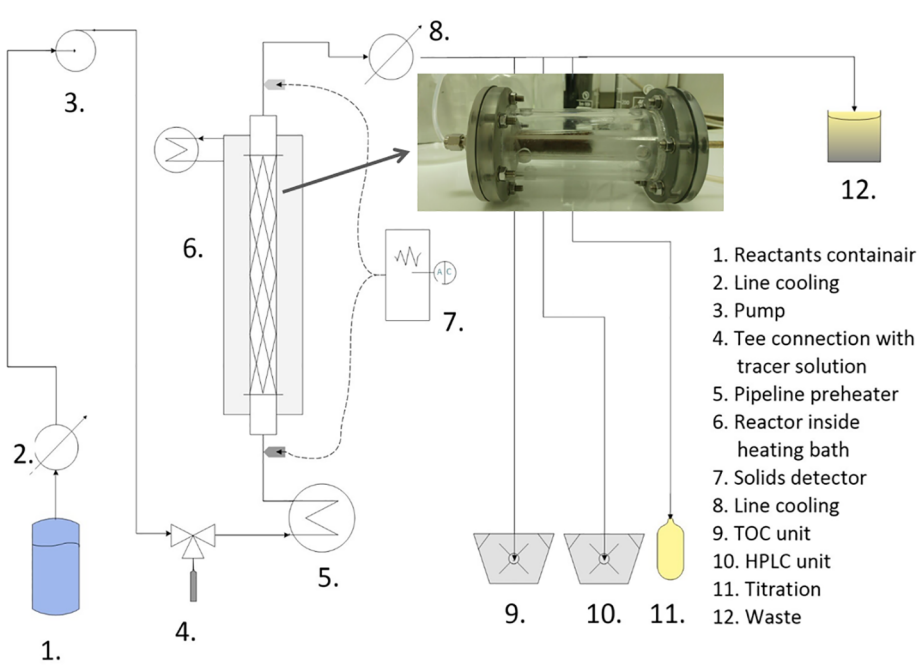

Fig. 2. Schematic diagram of the experimental set-up for the continuous flow CWPO of phenol. Inset: flow-through FBCR.

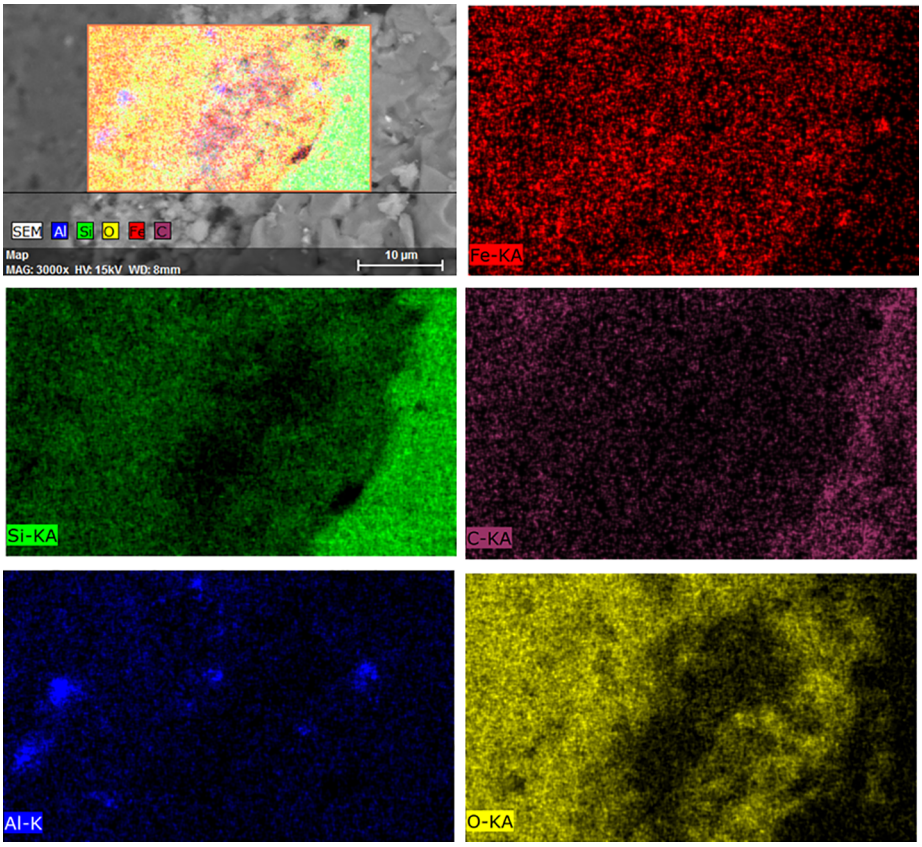

Fig. 3. Elemental mapping of Fe-ZSM-5/SiC catalyst by CVD for Fe, Si, C, Al and O by SEM-EDS.

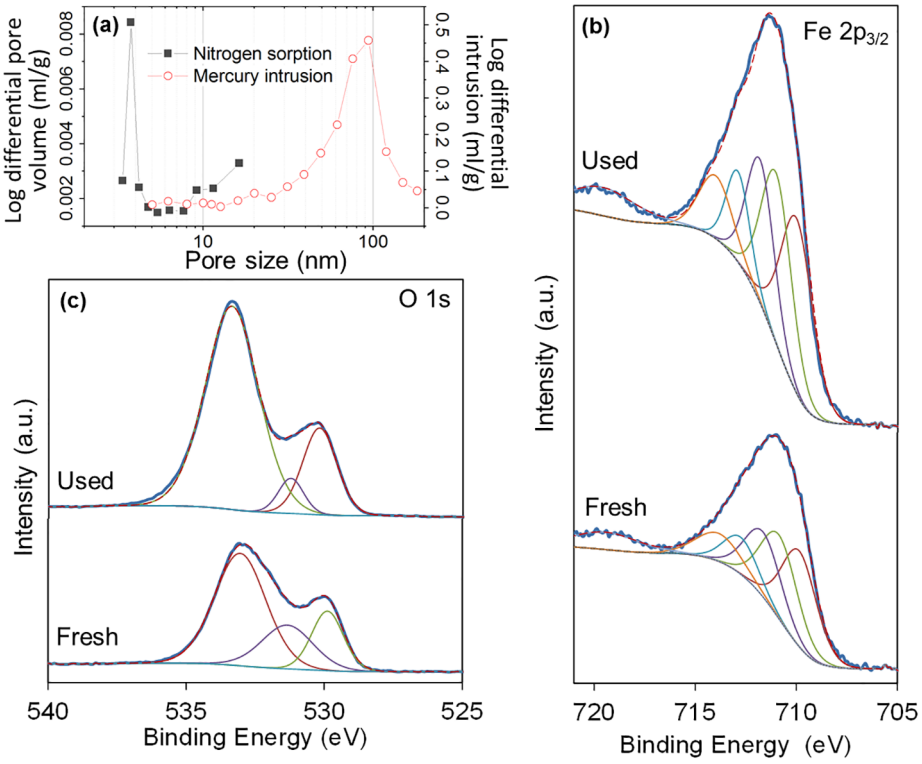

Fig. 4. (a) Meso-/macro-pore size distributions of Fe-ZSM-5/SiC by N_2 sorption and Hg porosimetry; XPS spectra of (b) Fe $2p_{3/2}$ and (c) O 1s of fresh/used (from the stability test) Fe-ZSM-5/SiC.

fitted for the fresh and used Fe-ZSM-5/SiC catalyst (Fig. 4b) according to the fitting parameters reported by Beisinger *et al* [56]. Fig. 4b shows a good fit for both the fresh and used catalyst when the spectral fitting parameters for Fe_2O_3 were used (Table S1), suggesting that Fe is in the 3^+ oxidation state in the two catalysts. Additionally, neither significant changes in Fe peaks nor Fe(0) (an absence of any peaks at 706.6 eV) are observed in either sample. In Fig. 4c, O 1s XPS profile shows three peaks in both the fresh and used catalyst. The peak at ~530.0 eV can be assigned to the lattice oxygen in the metallic Fe oxide structures, confirming the main presence of Fe_2O_3, the peaks at ~531.3 and ~533.0 eV could be assigned as surface hydroxyl or oxygen species, unsurprisingly, small changes in these peaks are observed in the used catalyst in comparison to the fresh one.

3.2. Effect of temperature on CWPO in FBCRs

At $F = 1\ \mathrm{ml\,min^{-1}}$, the effect of reaction temperature on the performance of Fe-ZSM-5/SiC FBCR in CWPO was investigated with findings shown in Fig. 5. Compared with cases at 25 and 40 °C, FBCR at 60 °C reached the steady state (defined as 10% statistical margin of error of the averaged phenol conversion) earlier, *i.e.* one hour after start-up. Under steady-state conditions, temperature showed significant influence on the H_2O_2 consumption in FBCRs (Fig. 5a). Specific rates of H_2O_2 decomposition were enhanced by increasing the system temperature, *i.e.* about 1.28×10^{-2}, 1.73×10^{-2} and $4.69 \times 10^{-2}\ \mathrm{mol_{H2O2}\,h^{-1}\,g_{Fe}^{-1}}$ for 25, 40 and 60 °C, respectively. Previous studies showed that the catalytic decomposition of H_2O_2 on iron oxides was related to the intrinsic rate of catalytic reactions and/or mass transfer rate of species from the bulk medium to the catalyst surface [57]. Since all experiments were carried out under the same hydrodynamic condition at a constant flow rate, the measured rate enhancement of H_2O_2 decomposition by increasing the temperature could be explained by the Arrhenius law. Fe-ZSM-5/SiC catalyst was active for converting phenol at temperatures studied with average steady-state conversions of 82, 90 and 99% at 25, 40 and 60 °C, respectively (Fig. 5b). H_2O_2 conversions did not correlate strongly to phenol conversions, since the conversion of phenol (into the first generation intermediates such as catechol and benzoquinone isomers, Fig. S5) is the first step of CWPO process [5–7,18,21,27,58], stoichiometrically requiring only 1–2 M equivalent of H_2O_2 [10,59]. The apparent activation energies (E_a) of Fe-ZSM-5/SiC catalyst for H_2O_2 decomposition and phenol oxidation were calculated according to Arrhenius equation (*i.e.* a plot of ln(TOF) *versus* T^{-1} giving a straight line, whose gradient can be used to determine E_a), as shown in Fig. 5c, the E_a value of Fe-ZSM-5/SiC for phenol degradation is *ca.* $3.7\ \mathrm{kJ\,mol^{-1}}$, lower than that reported for packed beds [60] and slurry reactors [24], also suggesting an improved catalytic system by the developed structured catalyst.

Blank experiments were carried out to evaluate (*i*) the adsorption of phenol on Fe-ZSM-5/SiC under flow conditions (without the oxidising agent of H_2O_2) and (*ii*) the phenol conversion caused by the non-catalytic oxidation of phenol by H_2O_2 under flow conditions (without the catalyst). Fig. 6a shows that phenol has a strong affinity towards Fe-ZSM-5/SiC catalyst, *e.g.* a maximum disappearance rate of about 55% was measured at 60 °C. As no H_2O_2 was present in blank experiments, the measured phenol disappearance was solely due to the adsorption of phenol on FBCR. Adsorption was favoured at the relatively low temperature of 25 °C, as expected. Negative values of phenol disappearance rate at 40 °C (in the saturated region of > 4 h) might be attributed to the desorption of adsorbed phenol molecules back to the flow, causing the excess mass balance between the inlet and outlet of FBCR. Blank flow-through experiments with an inert FBCR (with a SiC foam insert) and H_2O_2/phenol mixture (molar ratio = 14) were also carried out, showing that phenol degradation by H_2O_2 without catalyst was insignificant with an average phenol conversion of 16.5 ± 3.1% at 60 °C under the steady state (Fig. 6b). Based on the findings from blank experiments, Langmuir-Hinshelwood mechanism was very likely accountable for CWPO through FBCRs, in which oxidation reactions on the surface of Fe-ZSM-5/SiC catalysts prevailed.

Steady-state TOC conversions are presented as the inset in Fig. 5b, showing lower conversions of TOC than the corresponding phenol conversions due to the production of the first and secondary intermediates (*e.g.* acids such as maleic acid, oxalic acid, acetic acid and *etc.*) in CWPO of phenol [61]. For Fe-ZSM-5/SiC catalysts, under the condition used by this work, catechol and *p*-benzoquinone were detected as the main first generation intermediates at temperatures of 25 and 40 °C, contributing to TOCs of the effluent (Fig. S5), as well as the toxicity (half maximal effective concentration, EC_{50}, phenol (16.7) > catechol (8.32) > *p*-benzoquinone (0.1) [62]). For FBCR at 60 °C (Fig. S5), toxic intermediates were further decomposed into less toxic secondary acidic intermediates (*e.g.* $EC_{50,\ \mathrm{maleic\ acid}} \approx 247$, $EC_{50,\ \mathrm{oxalic\ acid}} > 450$ and $EC_{50,\ \mathrm{acetic\ acid}} \approx 130$ [62]), decreasing the pH of the catalytic system (pH = 3.5–4, under steady-state conditions, Fig. S6) and causing the leaching of Fe from FBCR (Table S2). Although Fe species in the aqueous solution may cause homogeneous Fenton-like reaction, a number of previous work have demonstrated that heterogeneous catalysis played the major role in mineralising phenol compared to the homogeneous catalysis (*e.g.* higher H_2O_2 degradation and TOC conversion can be observed through heterogeneous catalysis) [7,63].

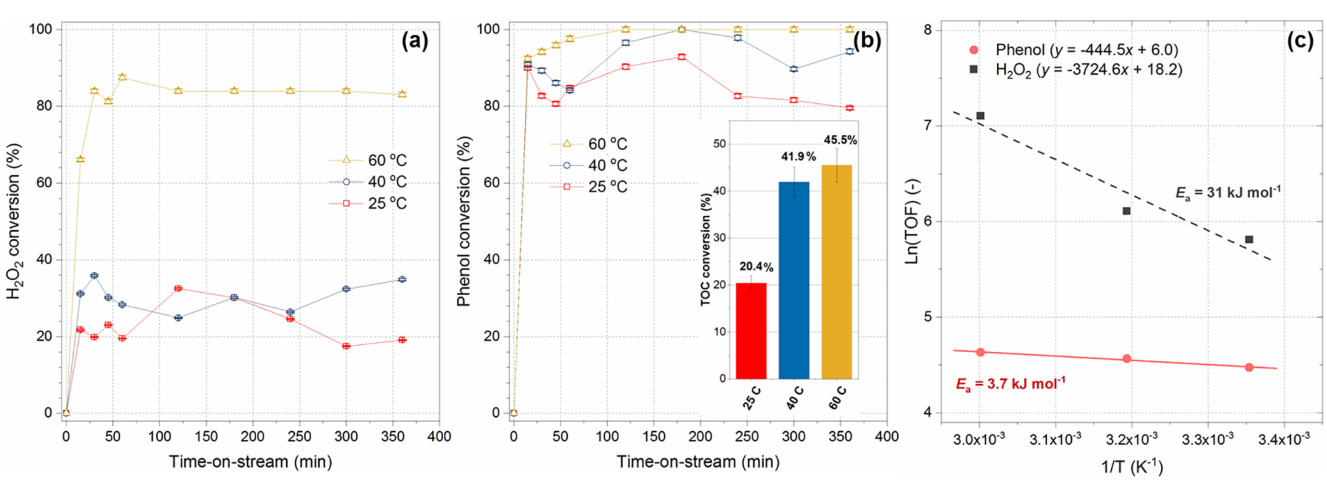

Fig. 5. Effect of the temperature on Fe-ZSM-5/SiC catalysed wet peroxide oxidation of phenol: (a) H_2O_2 consumption and (b) phenol conversions. Inset of (b): TOC conversions; (c) Arrhenius plots to determine the activation energy of catalytic H_2O_2 decomposition and phenol degradation in FBCRs (calculation of turnover frequency, TOF, is explained in the Supplementary Material. Conditions: $C_{\mathrm{phenol(0)}} = 100\ \mathrm{mg\,l^{-1}}$, molar ratio of H_2O_2 to phenol = 14, $F = 1\ \mathrm{ml\,min^{-1}}$. Error bars correspond to the average taken over at least three independent measurements.

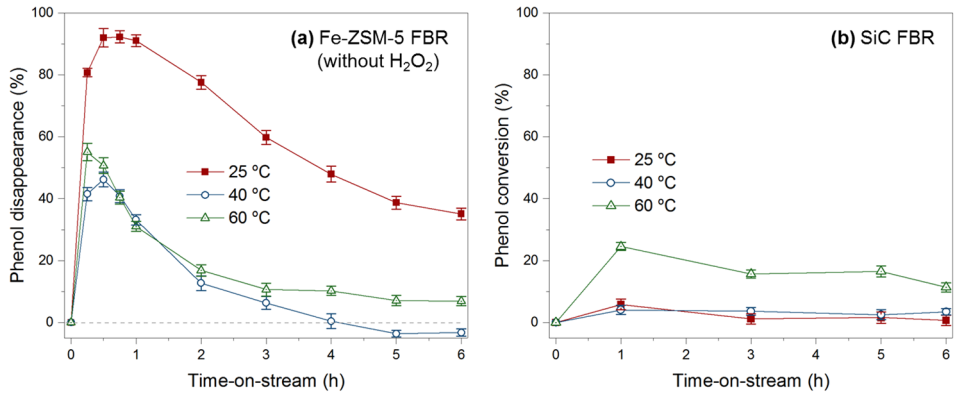

Fig. 6. Blank flow through experiments with (a) Fe-ZSM-5 FBCR without H_2O_2 and (b) SiC FBCR with H_2O_2/phenol mixture (molar ratio = 14). Conditions: $C_{phenol(0)}$ = 100 mg l^{-1}, F = 1 ml min^{-1}. Error bars correspond to the average taken over at least three independent measurements.

3.3. Effect of macromixing in FBCR on CWPO

The cellular structure of Fe-ZSM-5/SiC catalyst is expected to play a role in enhancing hydrodynamics (*i.e.* improved transport phenomena), and hence the apparent rate of phenol degradation. In comparison to packed bed configurations (Fe_2O_3 supported on MCM-41 [6] or SBA-15 [7]), Fe-ZSM-5/SiC catalyst achieved better TOFs than packed beds, *e.g.* 95.0 h^{-1} for Fe-ZSM-5/SiC *versus* 28.6 h^{-1} for Fe_2O_3@SBA-15 at *ca.* 60 °C and 1 ml min^{-1}. To investigate the effect of hydrodynamics of FBCR on catalytic reacting flows, CWPO of phenol aqueous solutions over Fe-ZSM-5/SiC FBCR was performed at 60 °C at flow rates of 0.5, 1 and 2 ml min^{-1}, respectively. It was found that the decomposition of H_2O_2 was favoured by low flow rates. Under steady state conditions as in Fig. 7a, the average conversion of H_2O_2 was measured to increase from about 59% to 88% by decreasing the flow rate from 2 to 0.5 ml min^{-1}. The pore-scale Reynolds numbers of the conditions used were estimated to be < 40 (Darcy flows), where the viscous force was prevailing [64,65]. Previously, we have shown that, for Darcy flows, foam supports were able to produce complex flow patterns at the millisecond scale and led to the axial and radial dispersion of species in and after cellular structures [66], as well as outperforming the conventional monoliths [35]. Therefore, the enhanced H_2O_2 conversions at low flow rates (*i.e.* by *ca.* 49% from 2 to 0.5 ml min^{-1}) could be explained by the improved liquid-to-solid transport by extending the residence time. The effect of flow rate on the conversion of phenol was minor as shown in Fig. 7b, showing that the first step of phenol degradation could be easily achieved by FBCR with > 59% H_2O_2 conversions (at 60 °C) under flow conditions.

Interestingly, the highest TOC conversion of 45.5% was achieved at 1 ml min^{-1}. A decrease in TOC conversion was measured by either increasing or decreasing of the flow rate, as the inset in Fig. 7b. In order to understand this phenomenon, pulse response experiments were carried out to characterise FBCR, gaining insight into the macromixing of FBCR on the continuous CWPO. Cumulative distribution functions ($F(t)$ curves), concentration-time curves and residence time distribution (RTD) curves ($E(t)$ curves) of FBCRs are shown in Fig. 8 (concentration profiles were smoothed using a fast Fourier transform filter to exclude noises). Other relevant parameters of RTD are summarised in Table 1.

Comparing normalised responses to pulse inputs, $F(t)$ curves at the inlet and outlet of FBCRs show that the tracer needed much more time to exit FBCR than that needed to enter the reactor (Fig. 8a and 8b). At 2 ml min^{-1}, it was observed that 80% $F(t)$ of tracer molecules spent 16 min or less in FBCR, while 27 min and 50 min were estimated for flow rates of 1 and 0.5 ml min^{-1}, respectively.

Calculated RTD curves at the outlet of FBCR as a function of time are shown in Fig. 8d for three flow rates. At 2 ml min^{-1}, $E(t)$ curve was narrow with reduced tailing, suggesting that FBCR behaved more like a non-ideal plug flow reactor (FB-PFR). At lower flow rates of 1 and 0.5 ml min^{-1}, $E(t)$ curves developed long tails with relatively long residence times. Especially, the RTD at 0.5 ml min^{-1} is very close to continuous stirred tank reactors (FB-CSTR), implying the possible existence of stagnant zones and/or recirculating zones in FBCRs under these flow rates. Theoretical space time (τ, or ideal residence time for a perfect plug flow reactor, PFR) of three cases is shown in Table 1, also as the vertical solid lines in Fig. 8d. It was found that all $E(t)$ curves arrived later than the expected τ, excluding the presence of stagnant fluids within FBCR. Therefore, the recirculation of fluid within the open-cell structure of FBCRs is likely to be responsible for the macromixing phenomena measured at 1 and 0.5 ml min^{-1}. Values of mean residence time (t_m) and variance (σ_t^2) were deduced from $E(t)$ for FBCR (as shown in Table 1). The value of σ_t^2 at 0.5 ml min^{-1} is one order of magnitude higher than those at 1 and 2 ml min^{-1}, suggesting a greater RTD's spread of fluid elements in the FBCR at 0.5 ml min^{-1} (*i.e.* similar to a not well mixed CSTR).

Based on the RTD characterisation of FBCR, ineffective phenol mineralisation at F = 0.5 ml min^{-1} (*i.e.* low TOC conversion of 33.1%)

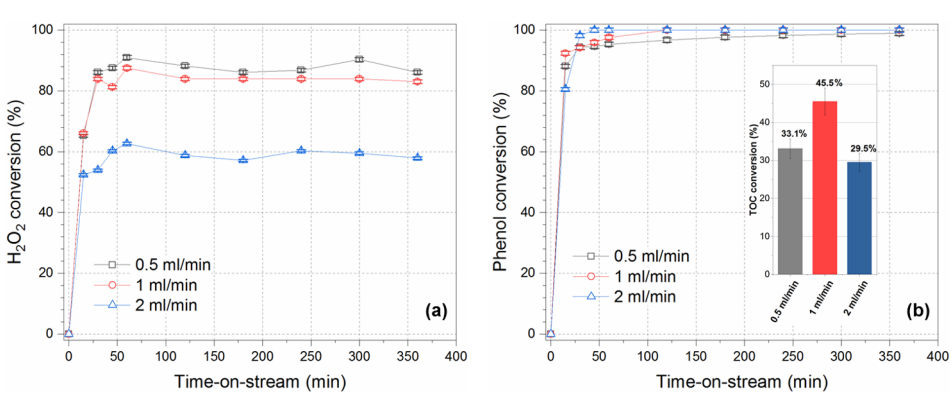

Fig. 7. Effect of the volumetric flow rate on Fe-ZSM-5/SiC catalysed wet peroxide oxidation of phenol: (a) H_2O_2 consumption and (b) phenol conversions. Inset: TOC conversions. Conditions: $C_{phenol(0)}$ = 100 mg l^{-1}, molar ratio of H_2O_2 to phenol = 14, T = 60 °C. Error bars correspond to the average taken over at least three independent measurements.

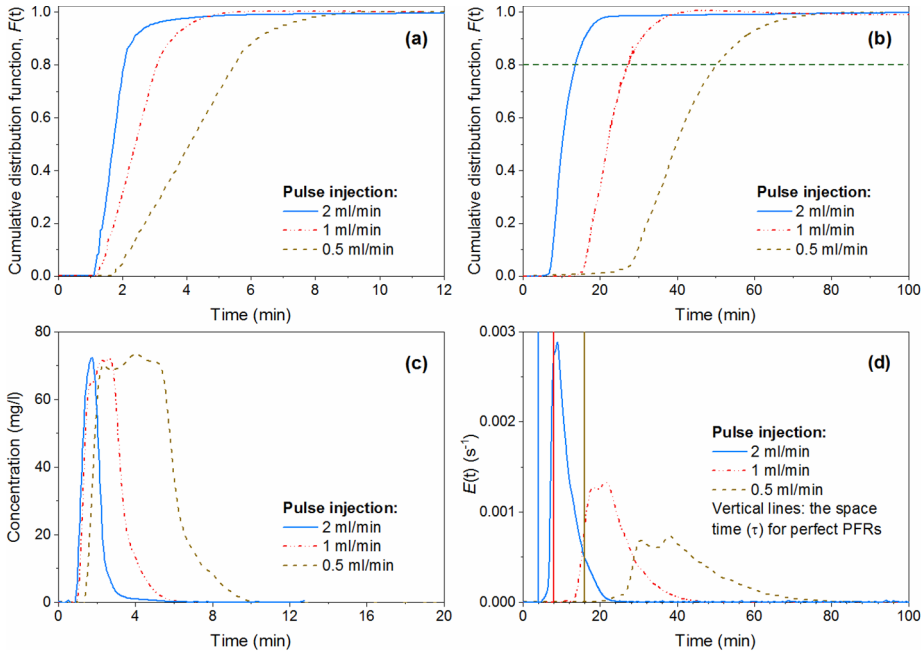

Fig. 8. (a) and (b) cumulative distribution functions ($F(t)$) at the inlet and outlet of FBCR; (c) concentration-time curves at the inlet of FBCR; (d) residence time distribution (RTD, $E(t)$) curves as the function of time for outlet of FBCR. Conditions: 4 wt% NaCl solution, injection volume = 2 ml, T = 60 °C.

Table 1
Space time, mean residence time and variance for FBCR at different flow rates.

Flow rate, ν [ml min^{-1}]	Space time, τ [min]	Mean residence time, t_m [min]	Variance, σ_t^2 [min^2]	σ^{2a} [−]
0.5	15.2	111	106	8.6×10^{-3}
1	7.6	41	28	1.6×10^{-2}
2	3.8	23	10	1.8×10^{-2}

[a] Dimensionless variance (σ^2) is calculated by $\sigma_t^2/(t_m^2)$.

could be explained due to the poor macromixing in FBCR, which could lead to the undesirable consumption of H_2O_2 in CWPO such as (*i*) the conversion of H_2O_2 into the less reactive hydroperoxy radical [10,12] and (*ii*) the consumption of hydroxyl radicals by the auto-scavenging reactions (with H_2O_2) [10]. For FB-PFR at 2 ml min^{-1}, short-circuiting fluid and channelling might exist, resulting in the short residence time, and hence low conversions of H_2O_2 and TOC (in comparison to FB-CSTR at 1 ml min^{-1}).

3.4. Catalyst longevity and repeatability of FBCRs in CWPO

The longevity and repeatability of Fe-ZSM-5/SiC catalysts under flow conditions were evaluated over six-hour cycles at 60 °C and 1 ml min^{-1} as shown in Fig. 9. For CWPO catalysed by Fe-ZSM-5/SiC FBCR, conversions of H_2O_2 and phenol stabilised at between 15 and 60 min after the start-up of the system and remained on same levels for the continuous run. The catalyst used in the longevity test was not fresh and bed washing using DI was performed between cycles. Catalyst activity at phenol conversions < 100% (*ca.* 93%, $C_{phenol(0)}$ = 1000 mg l^{-1}) was also checked showing no deactivation under the flow condition (Fig. S7). The catalyst longevity demonstrated by Fe-ZSM-5/SiC FBCR may have implications for relevant applications in practical settings where catalyst stability is often of paramount importance. Fe leaching as a function of the time-on-stream during the stability test was shown in Fig. S8, showing that the Fe leaching approached to a plateau at *ca.* 4.14 mg l^{-1} in the last two cycles. Post-reaction XPS analysis of the used Fe-ZSM-5/SiC catalyst (Fig. 4b and c) showed that the chemical state of iron species in the catalyst remained the same as that found for the fresh catalyst. Interestingly, the leaching of Fe species did not result in the significant drop in the catalytic activity of the developed FBCR, i.e. the conversions at the same time were shown to be relatively stable (Fig. 9). The origin of this phenomenon can be attributed to the leaching of inactive part of Fe or formation of the active clusters during the reaction [22], which requires further investigation.

4. Conclusions

Fe (0.2 wt%) supported on ZSM-5/SiC catalysts were prepared by chemical vapour deposition (CVD) with good dispersion of Fe_2O_3 in the ZSM-5 coating. Catalytic wet peroxide oxidation (CWPO) of phenol was carried out in Fe-ZSM-5/SiC based foam bed catalytic reactors (FBCRs) and showed good steady-state conversions of phenol (99%) and TOC (45.5%), as well as the TOF value of 95 h^{-1}, at the optimum condition of 60 °C and 1 ml min^{-1} (bed length = 80 mm).

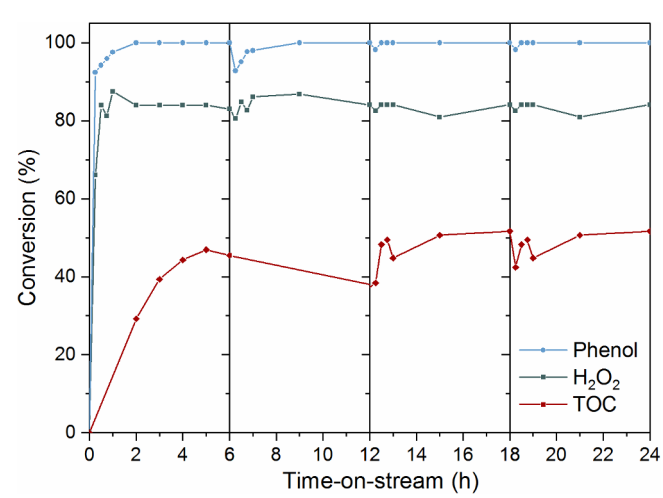

Fig. 9. Stability test of a Fe-ZSM-5/SiC catalyst for catalytic wet oxidation of phenol: conversions of phenol, H_2O_2 and TOC. Conditions: $C_{phenol(0)}$ = 100 mg l^{-1}, molar ratio of H_2O_2 to phenol = 14, T = 60 °C, F = 1 ml min^{-1}.

The characteristics of FBCRs were studied and research findings suggested that both hydrodynamics and residence time affected the decomposition of phenol significantly in FBCRs. RTD characterisation of the FBCR revealed that the reactor behaved differently before and after the transition flow rate of 1 ml min^{-1}, *e.g.* as a plug flow reactor at 2 ml min^{-1} and as a continuous stirred tank reactor at 0.5 ml min^{-1}. An optimum flow rate is necessary to operate the FBCR for continuous flow CWPO reactions, in which foam supports are able to maximise the macromixing as static mixers without compromising the residence time. In this work, it was anticipated that (*i*) short-circuiting and channelling at the high flow rate (2 ml min^{-1}) and (*ii*) recirculating zones at the low flow rate (0.5 ml min^{-1}) were plausible explanations for the reduced effective reactor volume, compromising the effective conversion of H_2O_2, and leading to less mineralisation of phenol in FBCRs. By comparing the effect of temperature and flow-rate on CWPO through FBCR, it was found that the effect of the system temperature on H_2O_2 decomposition was more profound than that by the flow-rate. H_2O_2 conversion was improved by *ca.* 180% by increasing the reaction temperature from 25 °C to 60 °C at 1 ml min^{-1}. Conversely, it was decreased by *ca.* 38% by increasing the flow-rate from 0.5 to 2 ml min^{-1} at 60 °C.

A longevity test of a Fe-ZSM-5/SiC based FBCR was carried out, showing a stable performance in terms of the phenol conversion. However, the Fe leaching from the Fe-ZSM-5/SiC catalyst (prepared by CVD) was observed, which is the concern for the further exploitation of the FBCR technology in practical settings. Further developments in the catalyst design are underway to address this issue.

Acknowledgements

The authors would like to thank the financial support from the Engineering and Physical Sciences Research Council for this research (EP/R000670/1). XO is grateful to the Guangzhou Elite Project scholarship and the CEAS postgraduate research scholarship, The University of Manchester. YJ thanks the financial support from the Liaoning Provincial Natural Science Foundation of China (20180510012) and the China Scholarship Council (CSC) for his visiting fellowship in the UK (file no. 201604910181). XF and YL also thank the Higher Education Innovation Funded 'Knowledge and Innovation Hub for Environmental Sustainability' at The University of Manchester for supporting YJ's visit to The University of Manchester. YY thanks the National Natural Science Foundation of China (21776106 and 21376101) and the Pearl River S&T Nova Program of Guangzhou (201610010171) for supporting her research.

Appendix A. Supplementary data

Supplementary data to this article can be found online at https://doi.org/10.1016/j.cej.2019.01.019.

References

[1] K. Mohanty, M. Jha, B.C. Meikap, M.N. Biswas, Preparation and characterization of activated carbons from Terminalia Arjuna nut with zinc chloride activation for the removal of Phenol from wastewater, Ind. Eng. Chem. Res. 44 (2005) 4128–4138, https://doi.org/10.1021/ie050162+.

[2] European Chemicals Bureau, Phenol – Summary Risk Assessment Report, 2006. < https://echa.europa.eu/documents/10162/1ca68f98-878f-4ef6-914a-9f21e9ad2234 > (accessed 13.12.18).

[3] A. Elena, C. Orbeci, C. Lazau, P. Sfirloaga, P. Vlazan, C. Bandas, I. Grozescu, Waste water treatment methods, in: W. Elshorbagy, R. Chowdhury (Eds.), Water Treatment, IntechOpen Limited, London, 2013, pp. 54–80, , https://doi.org/10.5772/53755.

[4] R. Andreozzi, V. Caprio, Amedeo Insola, Raffaele Marotta, Advanced oxidation processes (AOP) for water purification and recovery, Catal. Today 53 (1999) 51–59, https://doi.org/10.1016/S0920-5861(99)00102-9.

[5] Y. Yan, S. Jiang, H. Zhang, Efficient catalytic wet peroxide oxidation of phenol over Fe-ZSM-5 catalyst in a fixed bed reactor, Sep. Purif. Technol. 133 (2014) 365–374, https://doi.org/10.1016/j.seppur.2014.07.014.

[6] Y. Yan, X. Wu, H. Zhang, Catalytic wet peroxide oxidation of phenol over Fe 2 O 3/MCM-41 in a fixed bed reactor, Sep. Purif. Technol. 171 (2016) 52–61, https://doi.org/10.1016/j.seppur.2016.06.047.

[7] F. Martínez, J.A. Melero, J.Á. Botas, M.I. Pariente, R. Molina, Treatment of phenolic effluents by catalytic wet hydrogen peroxide oxidation over Fe_2O_3/SBA-15 extruded catalyst in a fixed-bed reactor, Ind. Eng. Chem. Res. 46 (2007) 4396–4405, https://doi.org/10.1021/ie070165h.

[8] S. Jiang, H. Zhang, Y. Yan, X. Zhang, Stability and deactivation of Fe-ZSM-5 zeolite catalyst for catalytic wet peroxide oxidation of phenol in a membrane reactor, RSC Adv. 5 (2015) 41269–41277, https://doi.org/10.1039/C5RA05039A.

[9] J. Zazo, J. Casas, A. Mohedano, J. Rodríguez, Catalytic wet peroxide oxidation of phenol with a Fe/active carbon catalyst, Appl. Catal. B Environ. 65 (2006) 261–268, https://doi.org/10.1016/j.apcatb.2006.02.008.

[10] S. Navalon, M. Alvaro, H. Garcia, Heterogeneous Fenton catalysts based on clays, silicas and zeolites, Appl. Catal. B Environ. 99 (2010) 1–26, https://doi.org/10.1016/j.apcatb.2010.07.006.

[11] P. Nidheesh, R. Gandhimathi, Trends in electro-Fenton process for water and wastewater treatment: an overview, Desalination 299 (2012) 1–15, https://doi.org/10.1016/j.desal.2012.05.011.

[12] A. Rey, M. Faraldos, J. Casas, J. Zazo, A. Bahamonde, J. Rodríguez, Catalytic wet peroxide oxidation of phenol over Fe/AC catalysts: influence of iron precursor and activated carbon surface, Appl. Catal. B Environ. 86 (2009) 69–77, https://doi.org/10.1016/j.apcatb.2008.07.023.

[13] J. Barrault, M. Abdellaoui, C. Bouchoule, A. Majesté, J. Tatibouët, A. Louloudi, N. Papayannakos, N. Gangas, Catalytic wet peroxide oxidation over mixed (Al–Fe) pillared clays, Appl. Catal. B Environ. 27 (2000) L225–L230, https://doi.org/10.1016/S0926-3373(00)00170-3.

[14] E. Guélou, J. Barrault, J. Fournier, J.-M. Tatibouët, Active iron species in the catalytic wet peroxide oxidation of phenol over pillared clays containing iron, Appl. Catal. B Environ. 44 (2003) 1–8, https://doi.org/10.1016/S0926-3373(03)00003-1.

[15] C.M. Domínguez, P. Ocón, A. Quintanilla, J.A. Casas, J.J. Rodriguez, Highly efficient application of activated carbon as catalyst for wet peroxide oxidation, Appl. Catal. B Environ. 140 (2013) 663–670, https://doi.org/10.1016/j.apcatb.2013.04.068.

[16] M. Munoz, Z.M. de Pedro, J.A. Casas, J.J. Rodriguez, Combining efficiently catalytic hydrodechlorination and wet peroxide oxidation (HDC–CWPO) for the abatement of organochlorinated water pollutants, Appl. Catal. B Environ. 150 (2014) 197–203, https://doi.org/10.1016/j.apcatb.2013.12.029.

[17] M. Munoz, F.J. Mora, Z.M. de Pedro, S. Alvarez-Torrellas, J.A. Casas, J.J. Rodriguez, Application of CWPO to the treatment of pharmaceutical emerging pollutants in different water matrices with a ferromagnetic catalyst, J. Hazard. Mater. 331 (2017) 45–54, https://doi.org/10.1016/j.jhazmat.2017.02.017.

[18] J. Melero, G. Calleja, F. Martínez, R. Molina, M. Pariente, Nanocomposite Fe_2O_3/SBA-15: an efficient and stable catalyst for the catalytic wet peroxidation of phenolic aqueous solutions, Chem. Eng. J. 131 (2007) 245–256, https://doi.org/10.1016/j.cej.2006.12.007.

[19] Y. Yan, S. Jiang, H. Zhang, Catalytic wet oxidation of phenol with Fe–ZSM-5 catalysts, RSC Adv. 6 (2016) 3850–3859, https://doi.org/10.1039/C5RA19832A.

[20] K. Fajerwerg, J. Foussard, A. Perrard, H. Debellefontaine, Wet oxidation of phenol by hydrogen peroxide: the key role of pH on the catalytic behaviour of Fe-ZSM-5, Water Sci. Technol. 35 (1997) 103–110, https://doi.org/10.2166/wst.1997.0096.

[21] Y. Yan, S.S. Jiang, H.P. Zhang, X.Y. Zhang, Preparation of novel Fe-ZSM-5 zeolite membrane catalysts for catalytic wet peroxide oxidation of phenol in a membrane reactor, Chem. Eng. J. 259 (2015) 243–251, https://doi.org/10.1016/j.cej.2014.08.018.

[22] O.P. Taran, S.A. Yashnik, A.B. Ayusheev, A.S. Piskun, R.V. Prihod'ko, Z.R. Ismagilov, V.V. Goncharuk, V.N. Parmon, Cu-containing MFI zeolites as catalysts for wet peroxide oxidation of formic acid as model organic contaminant, Appl. Catal. B Environ. 140–141 (2013) 506–515, https://doi.org/10.1016/j.apcatb.2013.04.050.

[23] O.P. Taran, A.N. Zagoruiko, A.B. Ayusheev, S.A. Yashnik, R.V. Prihod'ko, Z.R. Ismagilov, V.V. Goncharuk, V.N. Parmon, Wet peroxide oxidation of phenol over Cu-ZSM-5 catalyst in a flow reactor, Chem. Eng. J. 282 (2015) 108–115, https://doi.org/10.1016/j.cej.2015.02.064.

[24] O.P. Taran, A.N. Zagoruiko, A.B. Ayusheev, S.A. Yashnik, R.V. Prihod'ko, Z.R. Ismagilov, V.V. Goncharuk, V.N. Parmon, Cu and Fe-containing ZSM-5 zeolites as catalysts for wet peroxide oxidation of organic contaminants: reaction kinetics, Res. Chem. Intermed. 41 (2015) 9521–9537, https://doi.org/10.1007/s11164-015-1977-6.

[25] O.P. Taran, A.N. Zagoruiko, S.A. Yashnik, A.B. Ayusheev, A.V. Pestunov, I.P. Prosvirin, R.V. Prihod'ko, V.V. Goncharuk, V.N. Parmon, Wet peroxide oxidation of phenol over carbon/zeolite catalysts. Kinetics and diffusion study in batch and flow reactors, J. Environ Chem. Eng. 6 (2018,) 2551–2560, https://doi.org/10.1016/j.jece.2018.03.017.

[26] L. Shirazi, E. Jamshidi, M. Ghasemi, The effect of Si/Al ratio of ZSM-5 zeolite on its morphology, acidity and crystal size, Cryst. Res. Technol. 43 (2008) 1300–1306, https://doi.org/10.1002/crat.200800149.

[27] J. Botas, J. Melero, F. Martínez, M. Pariente, Assessment of Fe_2O_3/SiO_2 catalysts for the continuous treatment of phenol aqueous solutions in a fixed bed reactor, Catal. Today 149 (2010) 334–340, https://doi.org/10.1016/j.cattod.2009.06.014.

[28] S. Mitchell, N.-L. Michels, J. Pérez-Ramírez, From powder to technical body: the undervalued science of catalyst scale up, Chem. Soc. Rev. 42 (2013) 6094–6112, https://doi.org/10.1039/C3CS60076A.

[29] S. Jiang, H. Zhang, Y. Yan, Cu-MFI zeolite supported on paper-like sintered stainless fiber for catalytic wet peroxide oxidation of phenol in a batch reactor, Sep. Purif. Technol. 190 (2018) 243–251, https://doi.org/10.1016/j.seppur.2017.09.001.

[30] J. Wood, Monolith reactors for intensified processing in green chemistry, in: K. Boodhoo, A. Harvey (Eds.), Process Intensification for Green Chemistry: Engineering Solutions for Sustainable Chemical Processing, John Wiley & Sons Inc, New Jersey, 2013, pp. 175–197, , https://doi.org/10.1002/9781118498521.ch6.
[31] A. Montebelli, C.G. Visconti, G. Groppi, E. Tronconi, C. Cristiani, C. Ferreira, S. Kohler, Methods for the catalytic activation of metallic structured substrates, Catal. Sci. Technol. 4 (2014) 2846–2870, https://doi.org/10.1039/C4CY00179F.
[32] C. Duong-Viet, H. Ba, Z. El-Berrichi, J.-M. Nhut, M.J. Ledoux, Y. Liu, C. Pham-Huu, Silicon carbide foam as a porous support platform for catalytic applications, New J. Chem. 40 (2016) 4285–4299, https://doi.org/10.1039/C5NJ02847G.
[33] Y. Jiao, X. Fan, M. Perdjon, Z. Yang, J. Zhang, Vapor-phase transport (VPT) modification of ZSM-5/SiC foam catalyst using TPAOH vapor to improve the methanol-to-propylene (MTP) reaction, Appl. Catal. A Gen. 545 (2017) 104–112, https://doi.org/10.1016/j.apcata.2017.07.036.
[34] V. Hessel, D. Kralisch, N. Kockmann, T. Noël, Q. Wang, Novel process windows for enabling, accelerating, and uplifting flow chemistry, ChemSusChem 6 (2013) 746–789, https://doi.org/10.1002/cssc.201200766.
[35] M. Bracconi, M. Ambrosetti, O. Okafor, V. Sans, X. Zhang, X. Ou, C.P. Da Fonte, X. Fan, M. Maestri, G. Groppi, E. Tronconi, Investigation of pressure drop in 3D replicated open-cell foams: Coupling CFD with experimental data on additively manufactured foams, Chem. Eng. J. (2019), https://doi.org/10.1016/j.cej.2018.10.060.
[36] X. Ou, F. Pilitsis, N. Xu, S.F.R. Taylor, J. Warren, A. Garforth, J. Zhang, C. Hardacre, Y. Jiao, X. Fan, On developing ferrisilicate catalysts supported on silicon carbide (SiC) foam catalysts for continuous catalytic wet peroxide oxidation (CWPO) reactions, Catal. Today (2019), https://doi.org/10.1016/j.cattod.2018.06.033.
[37] S. Hajiesmaili, S. Josset, D. Bégin, C. Pham-Huu, N. Keller, V. Keller, 3D solid carbon foam-based photocatalytic materials for vapor phase flow-through structured photoreactors, Appl. Catal. A Gen. 382 (2010) 122–130, https://doi.org/10.1016/j.apcata.2010.04.044.
[38] S. Josset, S. Hajiesmaili, D. Begin, D. Edouard, C. Pham-Huu, M.-C. Lett, N. Keller, V. Keller, UV-A photocatalytic treatment of Legionella pneumophila bacteria contaminated airflows through three-dimensional solid foam structured photocatalytic reactors, J. Hazard. Mater. 175 (2010) 372–381, https://doi.org/10.1016/j.jhazmat.2009.10.013.
[39] R. Masson, V. Keller, N. Keller, β-SiC alveolar foams as a structured photocatalytic support for the gas phase photocatalytic degradation of methylethylketone, Appl. Catal. B Environ. 170–171 (2015) 301–311, https://doi.org/10.1016/j.apcatb.2015.01.030.
[40] D. Hao, Z. Yang, C. Jiang, J. Zhang, Synergistic photocatalytic effect of TiO_2 coatings and p-type semiconductive SiC foam supports for degradation of organic contaminant, Appl. Catal. B Environ. 144 (2014) 196–202, https://doi.org/10.1016/j.apcatb.2013.07.016.
[41] M.J. Ledoux, C. Pham-Huu, Silicon carbide: a novel catalyst support for heterogeneous catalysis, CATTECH 5 (2001) 226–246, https://doi.org/10.1023/A:1014092930183.
[42] L. Zhang, X. Liu, H. Li, H. Sui, X. Li, J. Zhang, Z. Yang, C. Tian, G. Gao, Hydrodynamic and mass transfer performances of a new SiC foam column tray, Chem. Eng. Technol. 35 (2012) 2075–2083, https://doi.org/10.1002/ceat.201200032.
[43] Y. Jiao, C. Jiang, Z. Yang, J. Zhang, Controllable synthesis of ZSM-5 coatings on SiC foam support for MTP application, Microporous Mesoporous Mater. 162 (2012) 152–158, https://doi.org/10.1016/j.micromeso.2012.05.034.
[44] Y. Liu, S. Podila, D.L. Nguyen, D. Edouard, P. Nguyen, C. Pham, M.J. Ledoux, C. Pham-Huu, Methanol dehydration to dimethyl ether in a platelet milli-reactor filled with H-ZSM5/SiC foam catalyst, Appl. Catal. A Gen. 409–410 (2011) 113–121, https://doi.org/10.1016/j.apcata.2011.09.035.
[45] X. Ou, S. Xu, J.M. Warnett, S.M. Holmes, A. Zaheer, A.A. Garforth, M.A. Williams, Y. Jiao, X. Fan, Creating hierarchies promptly: Microwave-accelerated synthesis of ZSM-5 zeolites on macrocellular silicon carbide (SiC) foams, Chem. Eng. J. 312 (2017) 1–9, https://doi.org/10.1016/j.cej.2016.11.116.
[46] Y. Jiao, C. Jiang, Z. Yang, J. Liu, J. Zhang, Synthesis of highly accessible ZSM-5 coatings on SiC foam support for MTP reaction, Microporous Mesoporous Mater. 181 (2013) 201–207, https://doi.org/10.1016/j.micromeso.2013.07.013.
[47] M.M. Elamin, O. Muraza, Z. Malaibari, H. Ba, J.-M. Nhut, C. Pham-Huu, Microwave assisted growth of SAPO-34 on β-SiC foams for methanol dehydration to dimethyl ether, Chem. Eng. J. 274 (2015) 113–122, https://doi.org/10.1016/j.cej.2015.03.118.
[48] Y. Liu, B. de Tymowski, F. Vigneron, I. Florea, O. Ersen, C. Meny, P. Nguyen, C. Pham, F. Luck, C. Pham-Huu, Titania-decorated silicon carbide-containing cobalt catalyst for Fischer-Tropsch synthesis, ACS Catal. 3 (2013) 393–404, https://doi.org/10.1021/cs300729p.
[49] Y. Liu, D. Edouard, D.L. Nguyen, D. Begin, P. Nguyen, C. Pham, C. Pham-Huu, High performance structured platelet milli-reactor filled with supported cobalt open cell SiC foam catalyst for the Fischer-Tropsch synthesis, Chem. Eng. J. 222 (2013) 265–273, https://doi.org/10.1016/j.cej.2013.02.066.
[50] Y. Jiao, X. Yang, C. Jiang, C. Tian, Z. Yang, J. Zhang, Hierarchical ZSM-5/SiC nanowhisker/SiC foam composites: Preparation and application in MTP reactions, J. Catal. 332 (2015) 70–76, https://doi.org/10.1016/j.jcat.2015.09.002.
[51] F. Pinna, Supported metal catalysts preparation, Catal. Today 41 (1998) 129–137, https://doi.org/10.1016/S0920-5861(98)00043-1.
[52] R. Takahashi, S. Sato, T. Sodesawa, M. Kato, S. Yoshida, Preparation of Cu/SiO_2 catalyst by solution exchange of wet silica gel, J. Sol-Gel Sci. Technol. 19 (2000) 715–718, https://doi.org/10.1023/A:1008779226170.
[53] C. Zhou, H. Zhang, Y. Yan, X. Zhang, Catalytic combustion of acetone over Cu/LTA zeolite membrane coated on stainless steel fibers by chemical vapor deposition, Microporous Mesoporous Mater. 248 (2017) 139–148, https://doi.org/10.1016/j.micromeso.2017.04.020.
[54] H.S. Fogler, Elements of Chemical Reaction Engineering, fifth ed., Prentice Hall, New Jersey, 1999.
[55] X. Ou, X. Zhang, T. Lowe, R. Blanc, M.N. Rad, Y. Wang, N. Batail, C. Pham, N. Shokri, A.A. Garforth, P.J. Withers, X. Fan, X-ray micro computed tomography characterization of cellular SiC foams for their applications in chemical engineering, Mater. Charact. 123 (2017) 20–28, https://doi.org/10.1016/j.matchar.2016.11.013.
[56] M.C. Biesinger, B.P. Payne, A.P. Grosvenor, L.W. Lau, A.R. Gerson, R.S.C. Smart, Resolving surface chemical states in XPS analysis of first row transition metals, oxides and hydroxides: Cr, Mn, Fe, Co and Ni, Appl. Surf. Sci. 257 (2011) 2717–2730, https://doi.org/10.1016/j.apsusc.2010.10.051.
[57] S.-S. Lin, M.D. Gurol, Catalytic decomposition of hydrogen peroxide on iron oxide: kinetics, mechanism, and implications, Environ. Sci. Technol. 32 (1998) 1417–1423, https://doi.org/10.1021/es970648k.
[58] S. Jiang, H. Zhang, Y. Yan, Catalytic wet peroxide oxidation of phenol wastewater over a novel Cu–ZSM-5 membrane catalyst, Catal. Commun. 71 (2015) 28–31, https://doi.org/10.1016/j.catcom.2015.08.006.
[59] F. Mijangos, F. Varona, N. Villota, Changes in solution color during phenol oxidation by Fenton reagent, Environ. Sci. Technol. 40 (2006) 5538–5543, https://doi.org/10.1021/es060866q.
[60] J. Guo, M. Al-Dahhan, Catalytic wet oxidation of phenol by hydrogen peroxide over pillared clay catalyst, Ind. Eng. Chem. Res. 42 (2003) 2450–2460, https://doi.org/10.1021/ie020344t.
[61] L. Liotta, M. Gruttadauria, G. Di Carlo, G. Perrini, V. Librando, Heterogeneous catalytic degradation of phenolic substrates: catalysts activity, J. Hazard. Mater. 162 (2009) 588–606, https://doi.org/10.1016/j.jhazmat.2008.05.115.
[62] A. Santos, P. Yustos, A. Quintanilla, F. Garcia-Ochoa, J. Casas, J. Rodriguez, Evolution of toxicity upon wet catalytic oxidation of phenol, Environ. Sci. Technol. 38 (2004) 133–138, https://doi.org/10.1021/es030476t.
[63] G. Calleja, J. Melero, F. Martinez, R. Molina, Activity and resistance of iron-containing amorphous, zeolitic and mesostructured materials for wet peroxide oxidation of phenol, Water Res. 39 (2005) 1741–1750, https://doi.org/10.1016/j.watres.2005.02.013.
[64] A. Della Torre, G. Montenegro, G. Tabor, M. Wears, CFD characterization of flow regimes inside open cell foam substrates, Int. J. Heat Fluid Flow 50 (2014) 72–82, https://doi.org/10.1016/j.ijheatfluidflow.2014.05.005.
[65] N. Dukhan, Metal Foams: Fundamentals and Applications, DEStech Publications Inc, Pennsylvania, 2013.
[66] X. Fan, X. Ou, F. Xing, G.A. Turley, P. Denissenko, M.A. Williams, N. Batail, C. Pham, A.A. Lapkin, Microtomography-based numerical simulations of heat transfer and fluid flow through β-SiC open-cell foams for catalysis, Catal. Today 278 (2016) 350–360, https://doi.org/10.1016/j.cattod.2015.12.012.